ChemComm

HIGHLIGHT

View Article Online
View Journal | View Issue

Cite this: *Chem. Commun.*, 2023, **59**, 8758

Growth mechanism of metal halide perovskite single crystals in solution

Mingquan Liao,[a] Mengling Xia,*[a] Yinsheng Xu,[a] Ping Lu[a] and Guangda Niu*[b]

Metal halide perovskite (MHP) single crystals (SCs) have been demonstrated to have significant potential in photodetectors and photovoltaic devices due to their exceptional optoelectronic properties. The most promising approach for large-scale fabrication of high-quality MHP SCs is the synthesis of MHP SCs in solution. To explain the mechanism and guide the crystal growth process, the classical nucleation-growth theory was established. However, it mainly focuses on zone melting systems and does not account for the interaction between perovskite and solvent. In this review, we specifically focus on the difference in the growth mechanism between MHP SCs in solution and traditional SCs synthesized by the melting method, which includes a discussion of the dissolution, nucleation, and growth processes. We then summarize recent advances in the preparation of MHP SCs based on the special growth mechanism of the perovskite system. The purpose of this review is to provide comprehensive information to offer targeted theoretical guidance as well as unified understanding for the preparation of high-quality MHP SCs in solution.

Received 8th May 2023,
Accepted 20th June 2023

DOI: 10.1039/d3cc02241b

rsc.li/chemcomm

1. Introduction

Metal halide perovskite (MHP) single crystals (SCs) have shown dramatic achievements in photodetectors and photovoltaic devices over recent years.[1–4] The unique antibonding orbital and remarkable defect tolerance characteristic of perovskites prompt low trap-state densities (10^7–10^9 cm^{-3}) and long carrier lifetimes (10^2–10^4 ns), which are comparable with the photovoltaic-quality silicon.[5–8] As the core component of an optoelectronic device, the inherent trait of MHP SCs rules the optoelectronic performance of the device. For example, the crystal structure and dimensions of MHP SCs directly determine the carrier mobility, while the bulk and surface defects determine the carrier lifetime, which directly affects the magnitude of the photocurrent in photodetectors.[9–12]

Despite the great application potential, fabrication of MHP SCs is still at the groping stage compared with the traditional SCs, such as $LuYSiO_5$:Ce (LYSO), $Bi_4Ge_3O_{12}$ (BGO), $Y_3Al_5O_{12}$

[a] *School of Materials Science and Engineering & State Key Laboratory of Silicate Materials for Architectures, Wuhan University of Technology, Wuhan 430070, China. E-mail: xiamengling@whut.edu.cn*
[b] *Wuhan National Laboratory for Optoelectronics (WNLO), Huazhong University of Science and Technology (HUST), Wuhan 430074, China. E-mail: guangda_niu@hust.edu.cn*

Mingquan Liao

Mingquan Liao received his BS degree from the College of Materials Science and Engineering, Wuhan Institute of Technology, in 2022. He is currently a master in the State Key Laboratory of Silicate Materials for Architectures, Wuhan University of Technology. His research work focuses on the growth of organic–inorganic hybrid metal halide perovskite single crystals in solution and their applications in radiation detectors.

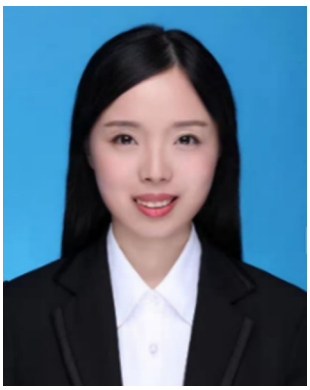

Mengling Xia

Mengling Xia is a professor at Wuhan University of Technology, China. She received her BS degree (2012) and PhD degree (2017) from Wuhan University of Technology. She was once a postdoc in Huazhong University of Science and Technology, China (Advisor: Prof. Jiang Tang). Her research focuses on the preparation of perovskite single crystals using a solution method and relevant mechanism analysis, and functional photoelectric devices based on perovskite materials.

(YAG), *etc.* Currently, there are various techniques available for fabricating MHP crystals, including melting–cooling growth, chemical vapor deposition (CVD), and solution-based approaches. Among these methods, the melting and cooling method is based on the principle of subjecting the raw material to a predetermined temperature gradient within a furnace. After melting in the heating zone, the raw material undergoes crystallization as it traverses the gradient zone and reaches the cooling zone. While the melting and cooling method facilitates the growth of large-sized crystals, it is primarily utilized for the preparation of all-inorganic MHP crystals.[13–15] As for the CVD method, the raw material is vaporized at elevated temperatures and subsequently deposited onto a substrate. By precisely adjusting the parameters such as temperature, pressure, and reaction time, the deposition of perovskite onto the substrate can be accurately controlled. However, it is usually applied for the preparation of the perovskite polycrystalline film.[16,17] In recent years, the solution-based approach has gained increasing popularity due to its inherent advantages of cost-effectiveness and ease of operation. Considering the various compositions and structures of metal halide perovskites, especially the organic–inorganic hybrid ones, the solution synthesis of MHP SCs has great potential for large-scale production.[18–22] At present, MHP SCs are prepared with various derivative solution-based methods, which is essentially the oversaturation driving by temperature (*e.g.* inverse temperature crystallization (ITC)[23,24]), precursor concentration (*e.g.* solvent evaporation method[25,26]) or solvent polarity (*e.g.* antisolvent vapor-assisted crystallization (AVC)[27,28]). By providing cost-effective and efficient approaches, these methods can facilitate the production of high-quality MHP SCs and potentially accelerate the commercialization of perovskite devices.

In order to guide the crystal growth process, classical theories and models have been established earlier, which mainly focus on zone melting systems without the involvement of solvent.[29,30] Later, LaMer's theories put forward the supplementary understanding of general nucleation and growth towards solution concentration, taking the role of solvents into consideration.[31,32] However, the interaction between perovskite and solvent, such as the complexation and decomplexation processes between metal ions and polar solvents, has not been taken into account. The complexation between solute and solvent affects the dissolution process, while decomplexation affects the subsequent nucleation rate and quantity. Therefore, in our opinion, dissolution, nucleation and growth, associated with the interaction between perovskite and solvent, are three key factors toward precise control over reproducibility and crystal quality of MHP SCs.

Growth of MHP SCs in solution has achieved great progress including exploring new categories, unfolding new mechanisms, and developing new technologies. Although several review articles have summarized the preparation principles and methods of MHP SCs, they mainly focus on the nucleation and growth mechanisms, the same as classical theories and models, without summarizing the unique growth theories for MHP systems, including the interaction between solvents and solutes.[33–36] In this review, we mainly describe the difference of growth mechanism between MHP SCs and traditional SCs by the melting method, and provide additional elucidation on precursor solution complexation. We hope that this review could offer comprehensive information aiming a targeted theoretical guidance as well as a unified understanding for the preparation of high-quality MHP SCs in solution.

2. Principles of nucleation and growth

2.1 Classical nucleation and growth

2.1.1 Nucleation. The process of nucleation of crystals is closely linked to both thermodynamics and kinetics. To understand the mechanism of nucleation, it is crucial to determine if it is thermodynamically favorable and if it occurs at a sufficient rate. In essence, these are the essential preconditions for gaining insight into the nucleation process. Classical nucleation theory is based on phase transitions without considering the interaction between solute and solvent. The homogenous nucleation and heterogeneous nucleation processes are depicted in Fig. 1a. According to classical theory, for a new spherical phase with radius r, the total free energy change (ΔG_r) of the system can be expressed as:

$$\Delta G_r = \Delta G_S + \Delta G_V = \pi r^2 \gamma_{GB} - \frac{4}{3}\pi r^3 \Delta G_V \quad (1)$$

where ΔG_V is the volumetric free energy per unit volume converted, and γ_{GB} is the specific surface free energy between the nucleus and the liquid. ΔG_V and γ_{GB} are fixed values at a given temperature. Eqn (1) reveals that the change in surface free energy (ΔG_S) and the change in volume free energy (ΔG_V) are proportional to r^2 and r^3, respectively. The interplay between surface and volume enthalpy explains the alteration of the overall free energy in the system, resulting in a critical nucleus radius (r_c) that corresponds to the maximum free energy of the system (Fig. 1b). At this point, the increment of Gibbs free energy is equal to one-third of the surface energy, that is, the difference in volume free energy between liquid and solid can only compensate two-thirds of the energy needed to form the critical surface of the crystal nucleus. The remaining one-third is made up by fluctuations in energy present in the liquid phase. Energy fluctuations require external energy input, such as increasing solution concentration and increasing temperature, *etc.* The surface energy becomes the predominant factor when r is less than r_c. Within this range, increasing the radius of the crystal nucleus raises the total free energy of the system, making the crystal nucleus unstable and easily dissolved in the solution. When r is larger than r_c, the volume free energy dominates. In this range, the free energy of the system is inversely proportional to the radius of the crystal nucleus, and the crystal nucleus can stably exist and grow up in the solution.

The nucleation barrier is reduced for the heterogeneous nucleation compared to homogeneous nucleation due to the reduced surface energy required. Heterogeneous nucleation forms at the interfaces of different phases. In particular, the nucleation sites emerge at the boundary between the liquid and another substrate, as shown in Fig. 1a. In this scenario, the formulation of interfacial enthalpy is altered, taking into account the interface energies of the liquid–solid (LS),

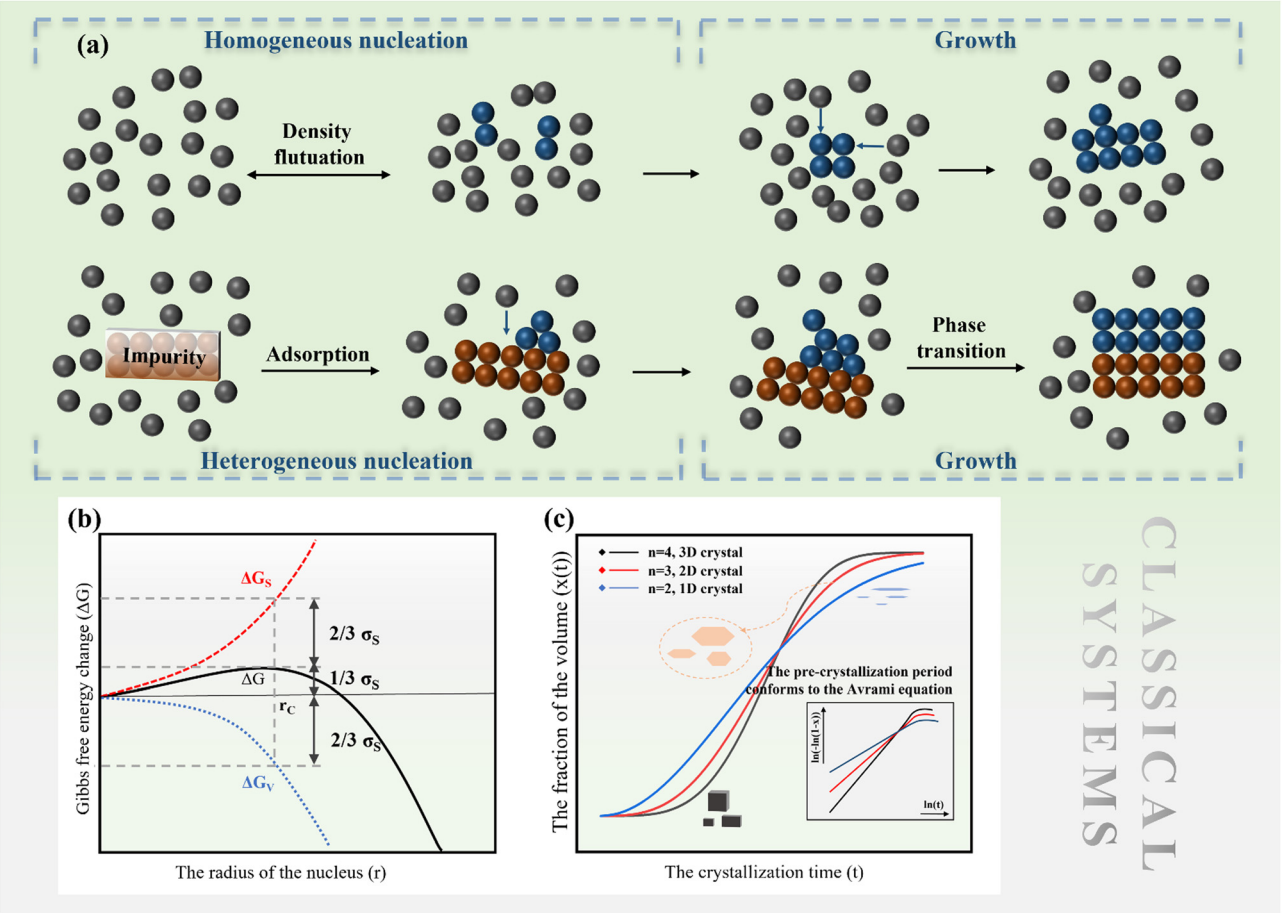

Fig. 1 (a) Nucleation and growth mechanisms in classical systems, (b) Gibbs energy change during the nucleation and growth process, and (c) growth models of 1D, 2D and 3D crystals, respectively. The inset is a function diagram with ln(*t*) as the independent variable in the JMA equation. The slope of the curve is closely related to the dimension of the crystal.

liquid–core (LC), and core–solid (CS) interfaces. Assuming that the shape of the crystal nucleus is a partial sphere with a radius r, the area of the liquid–crystal nucleus interface is A_{LC}, and the contact angle between the liquid and solid interface is θ, the enthalpy of the system forming the new phase can be expressed as:[37]

$$\Delta G_h = V\Delta G_V + \gamma_{LC}A_{LC} - \pi r^2\gamma_{LS}\cos\theta \quad (2)$$

where V is the volume of the crystal nucleus, and γ_{LC} and γ_{LS} are the interface energies of the liquid–crystal nucleus and liquid–substrate, respectively. As per eqn (2), the enthalpy of the system is dependent on the contact angle of the interface. Upon solving the critical enthalpy of both homogeneous and heterogeneous nucleation, $\Delta G_h^* = \Delta G_r^* f(\theta)$ can be obtained, where $f(\theta)$ is a coefficient that is solely related to the contact angle. This relationship reveals that as the contact angle decreases, the value of $f(\theta)$ also decreases, which results in a lower nucleation barrier. In other words, when the atomic arrangement of the nucleus and nucleator are similar, better wettability leads to more favorable nucleation. These findings underscore the crucial role that the interface plays in nucleation, and the importance of considering it when investigating liquid–solid phase transitions.

2.1.2 Growth. After the formation of a nucleus, crystals grow at a specific rate under controlled supersaturation conditions. The growth rate of crystals is believed to be strongly influenced by both the interface structure and atomic migration, as described by the theory of liquid–solid phase transitions. When the crystal phase has the same composition as the parent phase, the growth is primarily controlled by the interface. Particles near the interface only need to undergo an interface transition to attach to the surface of the crystal nucleus. However, when the structural composition of the two phases is different, solute atoms must diffuse to the interface between the new phase and parent phase, undergo interface transition, and then adhere to the surface of the new phase. In this scenario, diffusion is the main factor controlling the crystal growth. Based on the above discussion and further derivation, the growth rate of the crystal nucleus in the corresponding system can be determined. To more intuitively characterize the total crystallization rate of crystals, researchers often use the relationship between the fraction (x) of the volume of precipitated crystals in the initial volume of the parent liquid and the crystallization time (t). The Johnson–Mehl–Avrami (JMA) equation is a general formula that is widely accepted by researchers.

It can be expressed as:[38]

$$x = 1 - \exp\left(-\frac{\pi}{3} I U^3 t^4\right) \quad (3)$$

where I is the nucleation rate and U is the crystal growth rate at the interface of a single nucleus. Assuming that I and U are constant, the JMA equation can be expressed as the general formula ($x = 1 - \exp(-kt^n)$). The value of n in this equation is associated with the crystal's dimension, as illustrated in Fig. 1c. During the early growth stage, $x(t)$ changes only slightly and the curve is relatively flat. In the middle stage, the volume contains more nuclei, and the conversion rate increases sharply. In the later stage, as the solute is depleted, $x(t)$ approaches 100% and the curve plateaus. If the JMA equation is further simplified, a graph with $\ln(t)$ as the horizontal coordinate can be obtained, as shown in the inset of Fig. 1c. The slope of the curve corresponds to n, which remains constant in the early and middle growth stages, indicating that the JMA equation is a good fit for describing the crystal growth process. After the solute is depleted completely, the curve deviates significantly, suggesting that the JMA equation no longer provides an accurate description of the crystallization process.

2.2 Perovskite nucleation and growth

2.2.1 Dissolution. The classical theory of nucleation and growth primarily explains the process of pure crystals formation from the molten state to solidification. In the case of ionic crystals, the crystal is made up of ions, while covalent crystals are made up of molecules. These ions or molecules arrange themselves at specific intervals, creating short-range ordered and long-range disordered structures. When the energy input exceeds the nucleation barrier ($\Delta G < 0$), nucleation occurs, and the molten state begins to solidify. However, the perovskite solution system presents more complexities due to the interaction between the solute and solvent, compared to the classical system. Perovskites are generally completely ionized into ions in aqueous or water/acid mixture solvents. Nonetheless, in common polar organic solvents, such as *N*,*N*-dimethylformamide (DMF), dimethyl sulfoxide (DMSO), *N*-methylpyrrolidone (NMP), *etc.*, they can exist in various forms, including complexes or dissociated ions, non-dissociated molecules, or molecular clusters, as shown in Fig. 2a. For example, $MAPbI_3$ SCs were formed from dissociation of the intermediate complex $(MA^+)(PbI_3^-)_2DMF_2$.[39] In a simplified model, we consider a given solution system containing only one type of precursor molecules (X), which can exist in the form of (i) free precursor molecules "X", (ii) "X-cluster" nucleus, and (iii) solvated complex "X-xS" where one X is intermolecularly bonded with x solvent molecules (S) and has a complex binding energy.[40] The dynamics and equilibrium of these dissolution products affects the nucleation barrier and solute diffusion during the growth of MHP SCs.

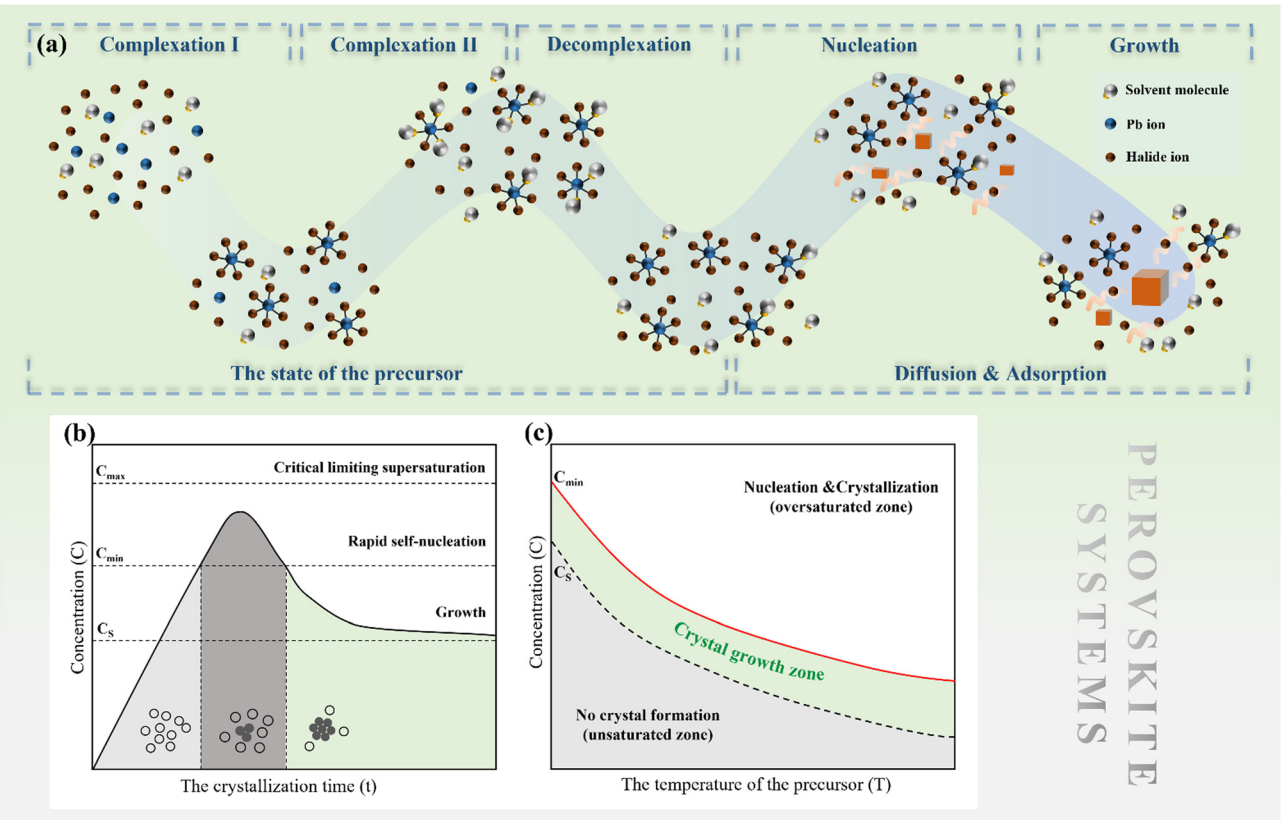

Fig. 2 (a) Nucleation and growth mechanism in the perovskite solution system, (b) LaMer's diagram approach to study the nucleation and growth of perovskite crystal in solution, and (c) evolution of unsaturated, saturated and oversaturated zone *versus* temperature.

2.2.2 Nucleation. The nucleation and growth processes of MHP SCs involve two main components: solute transport and interface adsorption. Similar to classical systems, the perovskite solution system also exhibits a nucleation barrier, and the nucleation rate and number of crystals are influenced by the oversaturation concentration of the solution. However, unlike classical systems, perovskite systems exhibit distinct nucleation and growth stages at different concentrations of the solution, as illustrated in Fig. 2b and c. LaMer's model has been utilized to describe the formation of monodisperse solutions.[31,32] Based on the saturation concentration (C_S) and minimum nucleation concentration (C_{min}), the solution can be divided into three regions.[41] When the concentration is below C_S, the perovskite system is stable and no nucleation occurs. In the range between C_S and C_{min}, there are limited nucleation sites in the system. Heterogeneous nucleation can occur, leading to a metastable state. When the concentration surpasses C_{min}, the nucleation rate becomes very rapid, resulting in an unstable state with a high number of nuclei. Temperature significantly influences the nucleation and growth of crystals in perovskite systems. The thermal convection gradient can induce entanglement defects and cracks in the perovskite SCs.[11,27] Recently, new experimental methods have been proposed to regulate the growth stage of crystals.[20,42–44] As depicted in Fig. 2, crystallization of the crystal growth zone occurs solely on existing nucleating seeds. By limiting the solution concentration to the optimal SC growth region using a small temperature gradient, high-quality $MAPbBr_3$ single crystals with dimensions of $47 \times 41 \times 14$ mm^3 have been prepared.[25] Another approach to regulate nucleation and growth during crystallization is the introduction of antisolvents, which can significantly affect the solution concentration and facilitate the preparation of different kinds of crystals.

The nucleation rate is determined by the concentration of critical nuclei in the parent phase per unit volume and the diffusion rate of atom to the nuclei. The widely accepted Arrhenius-type equation can well describe the formation rate of crystal nuclei (the number of crystal nuclei formed in unit volume of metastable solution within unit time).[45] The nucleation rate J can be expressed as:

$$J = \Lambda \exp\frac{-\Delta G}{k_B T} \tag{4}$$

where Λ is directly proportional to supersaturation, ΔG represents the energy barrier that must be overcome for the formation of critical crystal nuclei, k_B is Boltzmann constant and T is the absolute temperature. In addition to these factors, the participation of solvent in perovskite precursor solutions can also affect the nucleation barrier. Therefore, certain terminology related to nucleation and growth in such solutions needs to be revised, and the nucleation barrier has been modified accordingly to:[46]

$$\begin{aligned}\Delta G_{bulk} &= -\frac{4}{3}\pi r^3(\xi - \xi_A + k_B T \ln N_A) + \sigma \cdot 4\pi r^2 \\ &= \frac{16\pi}{3} \cdot \frac{\sigma^3}{(\xi - \xi_A + k_B T \cdot \ln(N_A))^2}\end{aligned} \tag{5}$$

The nucleation barrier can be characterized by the binding energy ξ of the precursor molecule in the cluster, the energy ξ_A of the precursor molecule, the mole fraction N_A of isolated A molecule, the surface energy σ of the cluster (based on a sphere model), and the nuclear radius r. To enhance the accuracy of this expression for the nucleation barrier, Wang *et al.* provided a more comprehensive description of the nucleation barrier for the MHP SCs system, expressed as:[40]

$$\Delta G_{bulk} = \frac{16}{3}\pi\sigma^3 \left(\xi - E_c - \xi_A + k_B T \ln \frac{1}{\frac{M_S^j}{M_A} - j^2 M_S^{j-1}} \right)^{-2} \tag{6}$$

where E_c is the complex binding energy, and M_S and M_A are the total molar concentration of solvent and precursor molecules. After modifying the nucleation barrier, classical nucleation theory is combined. This theory suggests that the nucleation of stable crystal nuclei can only occur when the radius of the crystal nucleus is larger than the critical radius of the crystal nucleus. The oversaturated solution can overcome the nucleation barrier and spontaneously precipitate the stable crystal nucleus. In the metastable region of perovskite solution system, although the precursor solution is oversaturated, there is still not enough energy to overcome the nucleation barrier. Since the rate of nucleation in the metastable region is close to zero, there is no additional nucleation. Therefore, there is potential in this region to prepare large size perovskite single crystals. In addition, in unstable regions, the nucleation rate of solution systems is very fast, which can limit the size of the grown crystals and lead to the formation of twin defects. These conclusions provide valuable guidance for the preparation of MHP SCs, and further exploration of the growth process can enhance our understanding of perovskite solution systems.

2.2.3 Growth. Compared to classical nucleation theory, the perovskite solution system for single crystal growth exhibits concentration fluctuations near the growth interface, which alternate between saturated and unsaturated conditions.[47–49] This phenomenon is attributed to the existence of two transition layers, namely the growth boundary layer and the diffusion boundary layer, in front of the crystal boundary. As the solute diffuses through the boundary layer to the growth interface during the growth of MHP SCs, the solute surrounding the single crystal is gradually depleted, resulting in a decrease in solution concentration around the crystal. Due to the impact of solution density and viscosity, solution convection experiences a certain delay. Solute in the diffusion layer fails to immediately reach the growth interface, leading to transient unsaturation at the growth interface of perovskite crystals. This alternating saturation and unsaturation phenomenon significantly influences crystal growth, and the solute concentration gradient is closely related to crystal growth rate. In metastable systems, the growth rate of crystals is governed by two factors: the transport rate of solute to the crystal interface and the deposition rate of solute at the interface. In the growth of MHP SCs, the rates of molecular adsorption and detachment of solutes play a crucial role in determining the crystal quality. To obtain high-quality MHP SCs, the deposition rate and diffusion rate need to reach a

dynamic equilibrium. The growth rate (Ψ) of perovskite crystals in solution systems can be described by the following equation:[40]

$$\Psi = \Gamma\nu\frac{\Delta G_C}{k_B T}\exp\frac{-\Delta G'}{k_B T} \quad (7)$$

where Γ represents the geometric factor, ν denotes the trial frequency, $\Delta G'$ indicates the free energy difference between the initial state and the activated state, and ΔG_C represents the free energy difference between the initial state and the crystalline state. As previously mentioned, crystal nucleation and growth processes are often intertwined, and different nucleation processes can affect crystal growth. LaMer's diagram provides a more detailed explanation of the growth process of single crystals, which involves prenucleation, nucleation, and growth as three stages of single crystal growth. To generate large perovskite single crystals, it is necessary to regulate both the nucleation and growth processes. Maintaining the solution concentration between C_S and C_{min} enables random nucleation and complete growth of the solution. According to the Ostwald ripening mechanism,[50,51] adding seed crystals at this stage can promote the growth of larger particles while dissolving smaller particles, thereby inhibiting nucleation and promoting the growth of single crystals.

An effective method for controlling the concentration of perovskite precursor involves the use of a room-temperature liquid diffusion separation-induced crystallization (LDSC) technique. This approach employs silicone oil to separate the solvent from the perovskite precursor, allowing for a balance between the accumulation and consumption of the precursor during the nucleation and growth stages. The LDSC method has proven to be highly successful in producing high-quality perovskite single crystals, thereby providing further evidence that maintaining the solution concentration within the metastable region (between C_S and C_{min}) enables stable growth of single crystals.[52] This technique offers significant potential for the growth of large, high-quality perovskite single crystals for use in optoelectronic applications.

3. Understanding the formation process of MHP SCs

It is highlighted that perovskite solution systems involve dissolution, which represents a significant departure from classical systems. The dissolution and growth processes involve complexation and decomplexation, which require careful consideration. Moreover, in classical theory, it is well-known that the interface plays a crucial role in crystal growth. The objective of this chapter is to explore the effects of these factors on nucleation and growth in perovskite solution systems, with the ultimate goal of providing a comprehensive understanding of the MHP SC growth mechanism.

3.1 A specific description of the precursor state

As discussed earlier, perovskite solution systems comprise of solute and solvent in various forms, where Pb^{2+} acts as a Lewis acid coordinated with a Lewis base. As shown in Fig. 3a, with the increase in MAI concentration in PbI_2 solution, the layered

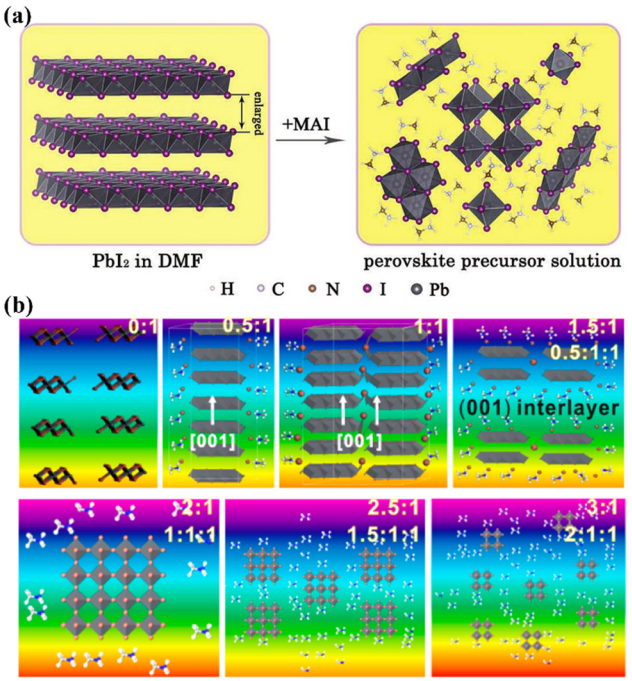

Fig. 3 (a) Schematic of the evolution of lead-iodine complexes after MAI addition.[53] Copyright 2019, Wiley-VCH Verlag. (b) Types of lead iodine complexes that may occur in precursors with different MAI/PbI2 mole ratios.[55] Copyright 2015, American Chemical Society.

structure of PbI_2 is further broken down to form various lead-iodine complexes,[53] which results in a series of changes in solution color with different species.[54] The addition of excess MAI can fill the empty coordination around Pb^{2+} and inhibit the formation of defective structures and the increase in colloid size (Fig. 3b).[55] As a result, the MAI-rich perovskite solution system can form an octahedral structure with high symmetry.[56] The choice of solvent also influences the crystal conversion, and the solvation ability of the solvent can be quantified using the Dn value.[57] Solvents with high Dn have a stronger binding with Pb^{2+} and thus higher stability of intermediates, making it difficult to separate Pb^{2+} from the coordinated solvent and affecting the crystallization kinetics of the perovskite solution system.

Short-term and long-term stability of precursors is critical in perovskite solution systems.[58–60] On the one hand, aging of the precursor affects the crystallinity of the MHP SCs. It has been reported that with the increase of aging resistance time of precursor solution, the colloid clusters in solution can maintain a larger volume for a long time.[61] Large colloidal clusters serve as nucleation sites, promoting crystal growth and improving the crystallinity of perovskite crystals.[61] On the other hand, organic solvents in the system can hydrolyze over time, leading to the destruction of the perovskite crystal structure. For instance, DMF hydrolyzed dimethylammonium ion (DMA^+) can replace MA^+ ions in the perovskite lattice.[62] Moreover, I^- in the precursor solution is easily oxidized to I_2, leading to an increase in the vacant coordination number of Pb^{2+} and an increase in defects in the generated perovskite.[63,64] Therefore, it is evident that the

precursor state is closely linked to the crystallization kinetics of perovskite crystals. By adjusting the solution components or external conditions, the perovskite solution system can remain in the appropriate stage for single crystal growth for an extended period, enabling the regulation of single crystal growth.

3.2 Control of complexation release crystallization

During the nucleation and growth of MHP SCs through the solution method, the process of decomplexation is also involved in addition to atomic diffusion and accumulation. Complexation and decomplexation has been widely used to slow down the crystallization rate of perovskite and control the crystallization quality.[65,66] In the case of $MAPbI_3$ SCs synthesized through ITC, organic solvent molecules bind to the octahedral lead iodine coordination. This leads to the formation of $(MA^+)(PbI_3^-)_2DMSO_2$, wherein the organic solvent occupation regulates the nucleation and growth of perovskite crystals. As depicted in Fig. 4a and b, when PbI2, MAI, and DMSO are mixed, an intermediate complex (INT-7) is initially formed. As the temperature increases to 100 °C, the organic complex gradually dissociates from the lead iodine octahedron, which helps to control nucleation.[39] By regulating the nucleation and growth of perovskite in this way, the size and dimensions of the crystals can be further adjusted.

After gaining an understanding of how organic solvents impact perovskite crystal nucleation and growth, some researchers have proposed using organic macromolecules in the precursor solution of perovskite to control nucleation and crystal growth. Initially, this method involved adding supplementary additives to adjust the active layer performance of perovskite solar cells.[67–71] In recent studies, this strategy has also been implemented for the production of large-sized MHP SCs.[65,66,72] Typically, organic macromolecules or polymers with specific functional groups are employed to regulate the nucleation and growth of MHP SCs. Examples of such functional groups include the carbon–oxygen bond in polyether (ester)-based molecules and the fluorine ion group,[68] as well as the carbon–nitrogen bond in polymethyl methacrylate-acrylamide and 2-cyanoacrylate.[69,70] These additives are broadly categorized into three groups based on their functional groups: S-donors, O-donors, and N-donors, with varying coordination capabilities. The coordination strength of the donors with Pb^{2+} follows the order: S-donor > O-donor > N-donor. Due to the unique coordination properties of these ionic groups, coordination complexes such as $(MA^+)_2(Pb_3I_8^{2-})DMSO_2$ can be

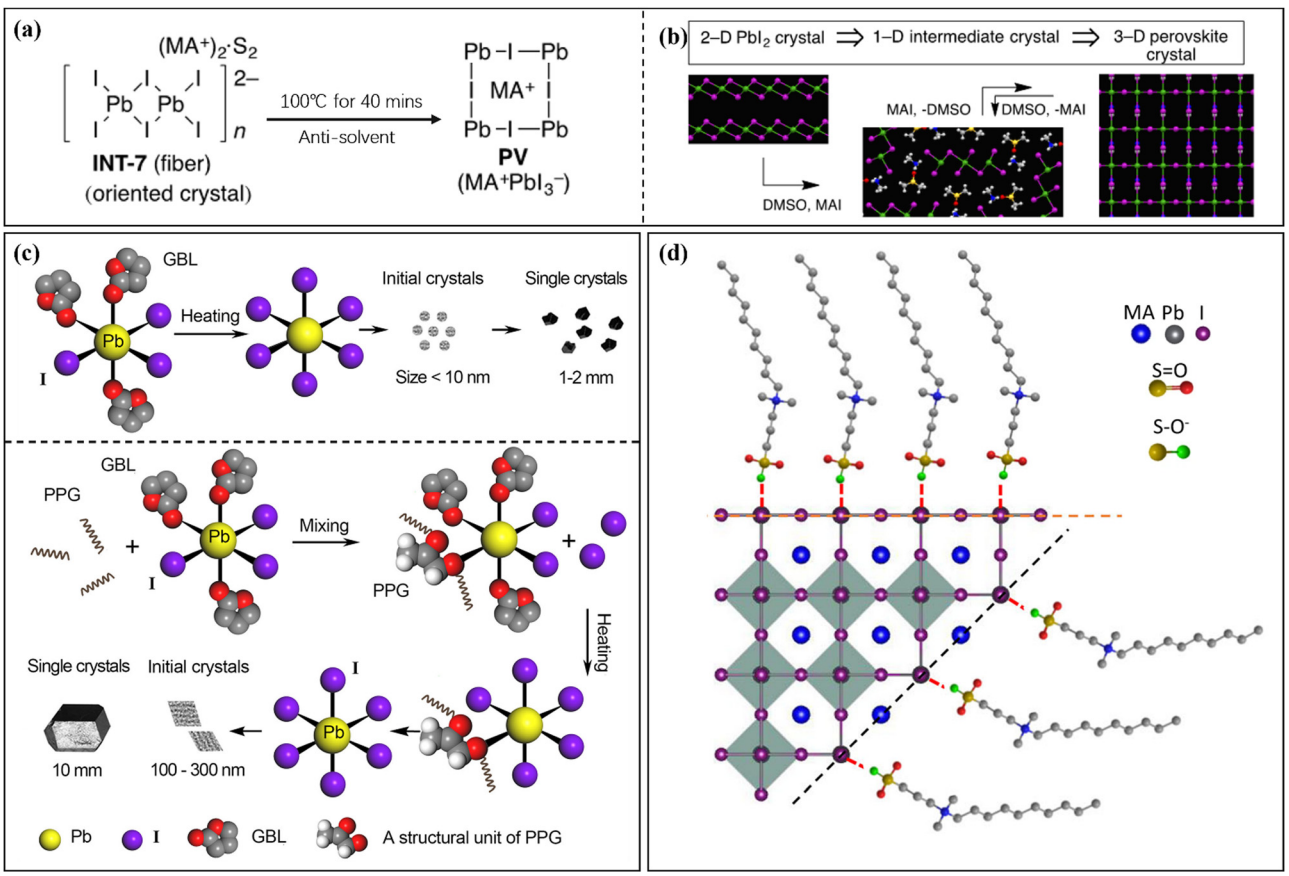

Fig. 4 Complex transformation of the $MAPbI_3$ perovskite single crystal (a) after adding organic solvent (DMSO).[39] Copyright 2015, American Chemical Society. (b) Schematic diagram of the crystal structure during the transformation process.[39] Copyright 2015, American Chemical Society. (c) Schematic diagram of crystallization mechanism after adding additive (PGG).[66] Copyright 2021, Springer Nature. (d) DPSI absorption differences on crystal planes with different Pb2+ densities.[65] Copyright 2021, Springer Nature.

formed.[39] Furthermore, the presence of certain groups and carbon chain length characteristics in the additive contributes to the hydrophobicity and stability of the active layer in perovskite solar cells.[73–75] As shown in Fig. 4c, the conventional solvent (*e.g.* GBL) can form Pb-solvent complexes at room temperature, while polypropylene glycol (PPG) that contains oxygen groups can coordinate with Pb^{2+}.[66] At low temperature, the solution primarily exists in a complex form, and as the temperature increases, dissociation between the groups of this complex occurs, leading to improved ion diffusion efficiency in the precursor solution. This efficient transfer of ions to the growth interface layer enables the solution to quickly and stably reach a saturated state, which is the fundamental principle behind polymer-assisted controlling nucleation. The dissociation under higher temperature conditions also serves as the driving force for crystal nucleation. Furthermore, studies have demonstrated that crystal faces with different Pb^{2+} densities grow at different rates, with crystal faces exhibiting lower Pb^{2+} density growing faster but being more prone to disappearing (Fig. 4d).[65] This steric hindrance effect of the polymer impedes the diffusion of ions to the perovskite surface, leading to varying crystal face growth rates. Understanding these mechanisms will aid in the selection of macromolecules and provide more possibilities for preparing large-sized SCs.

3.3 Interfacial extra tensile elastic stress induced crystallization

Solute deposition during crystal growth is a necessary process for the formation of crystal nuclei. The assembly of solute molecules or atoms is a complex process that involves interfacial dynamics.[76,77] Crystal growth is essentially a transport process that involves mass, heat, and momentum. A solute boundary layer is assumed to exist on the surface of the crystal, with an ideal fluid outside this boundary layer. Mass and heat transport outside the boundary layer are mainly governed by convection outside the boundary layer, while inside the layer, convection and diffusion play a more significant role due to the presence of large concentration and temperature gradients. This theory provides a basis for understanding the interface's role in the growth of MHP SCs. Differs from the liquid–solid interface in classical theory system, the surface tension generated by the solution–air interface plays a critical role in MHP SCs nucleation and growth.[46,78–80] As depicted in Fig. 5a and b, surface molecules experience strain owing to the presence of surface tension. Consequently, crystals suspended at the solution surface exhibit faster growth rates at the edges, resulting in a length-to-diameter ratio exceeding unity. The solvated surface molecules exist in a strained state with low energy. Crystal nuclei continue to grow on the surface of the solution until they reach a size at which surface tension no longer supports their buoyancy. Combined with eqn (5), the nucleation barrier of the solution–air interface layer can be expressed as:[46]

$$\Delta G_{\text{Surface}} = \frac{16\pi}{3} \cdot \frac{\sigma^3}{(\varepsilon + \varepsilon_{\text{surf}} - \varepsilon_{\text{A}} + k_{\text{B}}T \cdot \ln(N_{\text{A}}))^2} \quad (8)$$

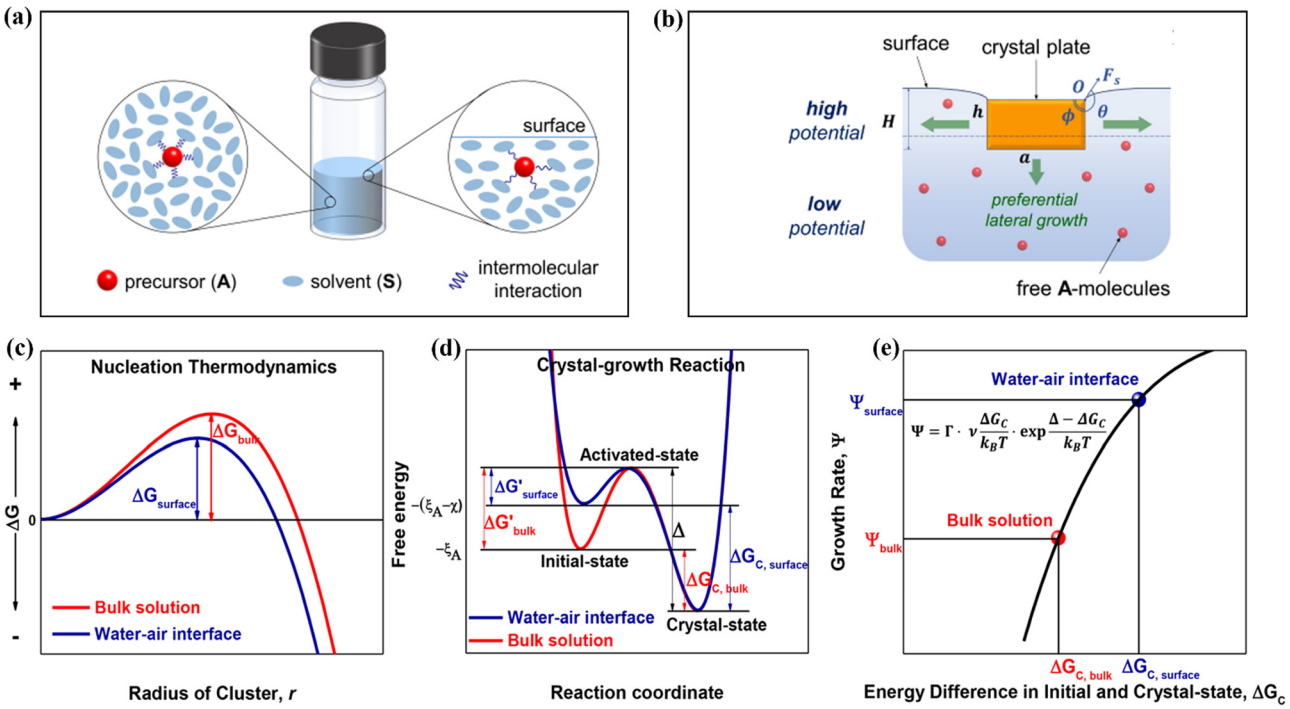

Fig. 5 (a) Schematic diagram of changes in molecular interaction energy in bulk solution (left) and surface layer (right).[46] Copyright 2017, American Chemical Society. (b) Schematic of the growth of a crystal in a floating state.[46] Copyright 2017, American Chemical Society. (c) Nucleation barrier at different interfaces.[40] Copyright 2018, American Chemical Society. (d) Initial state free energy, excited state free energy and crystalline free energy at different interfaces.[40] Copyright 2018, American Chemical Society. (e) Crystal growth rates corresponding to nucleation barriers at different interfaces.[40] Copyright 2018, American Chemical Society.

where ε_{surf} is the elastic energy of each molecule A in the solution–air interface layer that is related to the surface tension. As surface tension increases, ε_{surf} also increases. By comparing the nucleation barrier in bulk solution (eqn (5)), it can be observed that the nucleation barrier in the surface layer is lower, leading to a faster nucleation rate, which is further supported by eqn (6). Fig. 5c and d illustrate that the surface energy at the solution–air interface results in a higher initial energy of the precursor molecules. Due to the smaller free energy difference ($\Delta G'$) between the initial state and the active state, and the larger free energy difference (ΔG_C) between the initial state and the crystalline state, crystals grow much faster at the solution–air interface than in the out-of-plane direction, thereby exhibiting strong anisotropic growth rates (Fig. 5e).[40,81] Utilizing surface tension on the solution–air interface could facilitate the synthesis of low-dimensional MHP SCs.

Conclusions

MHP SCs have garnered significant attention as a new generation of photoelectric materials due to their exceptional properties. The solution method is a cost-effective and efficient approach for obtaining MHP SCs, and this review delves into the nucleation and growth mechanism, exploring the commonalities and differences between classical systems and perovskite solution systems. Unique aspects of perovskite solution systems, such as intermolecular complexation and decomplexation of precursor molecules, have a profound influence on nucleation and growth. The size of the colloid clusters is reflected in the deposition rate of the solute. The addition of large molecules containing specific groups can effectively modulate the ratio of the diffusion rate to deposition rate, optimizing the system for ideal crystal growth. By manipulating the components or external factors in the perovskite solution system, the system can be maintained in a suitable non-nucleated state for an extended period, facilitating the growth of large-sized single crystals. Nevertheless, there are still many aspects that need additional work, including but not limited to:

(1) Establishing comprehensive growth model of MHP SCs

The investigation of the growth mechanisms of MHP is still in its nascent stage compared to the traditional oxide single crystals. Although the LaMer's diagram has been employed to elucidate the nucleation and growth processes, the interaction between perovskite and solvent remains inadequately illustrated. Besides, molecular dynamics, phase-field, and thermal field simulations have been sufficiently applied in investigating the growth mechanisms of conventional crystals, such as SiC and NaCl. ANSYS Fluent, focusing on the sedimentary growth of the vapor phase, has been used to calculate heat and mass transfer during the growth process of MHP. However, there remains a dearth of studies on the theoretical simulations within perovskite solution systems, particularly in the realm of theoretical simulations pertaining to nucleation and growth processes. To provide a more comprehensive understanding of the growth mechanism in MHP, the development of a thorough theoretical model is urgently required.

(2) Real-time monitoring of the growth process of MHP SCs

Conventional real-time monitoring methods predominantly concentrate on crystal size and visual characteristics. However, when investigating the mechanism of MHP SCs, elucidating the nucleation and growth processes within the perovskite solution system, encompassing the underlying pathways of crystal formation and the structure of colloidal clusters, poses significant challenges for direct confirmation. Consequently, the advancement of a technique capable of real-time monitoring of solute diffusion and deposition processes has potential to expedite the progress in MHP SC development.

(3) Exploring new solvent and additives for the growth of MHP SCs

The conventional solution-based method presents challenges in achieving the growth of large-sized MHP SCs, and the process itself is time-consuming, significantly restricting the potential applications of MHP SCs. Moreover, even slight temperature fluctuations within the solution can result in undesirable outcomes, such as nucleation disorders and crystal defects. To address this issue, various passivation strategies have been proposed, as outlined in Section 3.2. However, the currently employed additives still fail to effectively control the crystal growth process. Therefore, there is an urgent demand for exploring more suitable new solvent and functional additives to facilitate the production of large-sized MHP SCs with minimal defects.

(4) Post-processing of MHP SCs

MHP SCs exhibit the absence of grain boundaries (GBs), which effectively mitigates non-radiative recombination at interfaces. While the elimination of GBs can diminish bulk phase defects in MHP SCs, the presence of surface defects, such as dangling bonds and dislocations, can significantly affect the optical and electrical properties of the MHP SCs. Furthermore, the residual organic solvents tend to accumulate on the crystal surface and can strongly interact with water molecules in humid environments, resulting in poor surface morphology. Consequently, effective post-treatment processes are of utmost importance to mitigate the impact of surface defects. Post-treatment has been a very important research direction in commercial single crystal, such as monocrystalline silicon and cadmium zinc telluride, but it has not been paid attention to in MHP SCs. Notably, the polishing method, including chemical polishing and mechanical polishing, and the selection of suitable polishing agents represent critical steps warranting meticulous attention in the post-treatment process.

Conflicts of interest

There are no conflicts to declare.

Acknowledgements

The authors acknowledge the financial support of the National Natural Science Foundation of China (62275206, U2241236, 61905082, 61975156) and State Key Laboratory of Silicate Materials for Architectures (Wuhan University of Technology) (SYSJJ2021-01).

References

1 L. Lei, Q. Dong, K. Gundogdu and F. So, *Adv. Funct. Mater.*, 2021, **31**, 2010144.
2 J. A. Steele, W. Pan, C. Martin, M. Keshavarz, E. Debroye, H. Yuan, S. Banerjee, E. Fron, D. Jonckheere, C. W. Kim, W. Baekelant, G. Niu, J. Tang, J. Vanacken, M. Van der Auweraer, J. Hofkens and M. B. J. Roeffaers, *Adv. Mater.*, 2018, **30**, 1804450.
3 J. Jiang, M. Xiong, K. Fan, C. Bao, D. Xin, Z. Pan, L. Fei, H. Huang, L. Zhou, K. Yao, X. Zheng, L. Shen and F. Gao, *Nat. Photonics*, 2022, **16**, 575–581.
4 D. Corzo, T. Wang, M. Gedda, E. Yengel, J. I. Khan, R. Li, M. R. Niazi, Z. Huang, T. Kim, D. Baran, D. Sun, F. Laquai, T. D. Anthopoulos and A. Amassian, *Adv. Mater.*, 2022, **34**, 2109862.
5 G. W. Kim and A. Petrozza, *Adv. Energy Mater.*, 2020, **10**, 6.
6 H. Tan, F. Che, M. Wei, Y. Zhao, M. I. Saidaminov, P. Todorović, D. Broberg, G. Walters, F. Tan, T. Zhuang, B. Sun, Z. Liang, H. Yuan, E. Fron, J. Kim, Z. Yang, O. Voznyy, M. Asta and E. H. Sargent, *Nat. Commun.*, 2018, **9**, 3100.
7 I. du Fosse, J. T. Mulder, G. Almeida, A. G. M. Spruit, I. Infante, F. C. Grozema and A. J. Houtepen, *J. Am. Chem. Soc.*, 2022, **144**, 11059–11063.
8 W. Chu, Q. Zheng, O. V. Prezhdo, J. Zhao and W. A. Saidi, *Sci. Adv.*, 2020, **6**, eaaw7453.
9 J. Siekmann, S. Ravishankar and T. Kirchartz, *ACS Energy Lett.*, 2021, **6**, 3244–3251.
10 E. Aydin, M. De Bastiani and S. De Wolf, *Adv. Mater.*, 2019, **31**, 20.
11 L. K. Ono, S. Z. Liu and Y. B. Qi, *Angew. Chem., Int. Ed.*, 2020, **59**, 6676–6698.
12 C. W. Li, Z. N. Song, D. W. Zhao, C. X. Xiao, B. Subedi, N. Shrestha, M. M. Junda, C. L. Wang, C. S. Jiang, M. Al-Jassim, R. J. Ellingson, N. J. Podraza, K. Zhu and Y. F. Yan, *Adv. Energy Mater.*, 2019, **9**, 9.
13 Y. Cai, S. Yan, X. Du, T. Lin, Y.-J. Lin, L. Qiu and W. Wang, *Adv. Funct. Mater.*, 2023, **33**, 2211191.
14 V. B. Mykhaylyk, M. Rudko, H. Kraus, V. Kapustianyk, V. Kolomiets, N. Vitoratou, Y. Chornodolskyy, A. S. Voloshinovskii and L. Vasylechko, *J. Mater. Chem. C*, 2023, **11**, 656–665.
15 Q. Sun, B. Xiao, L. Ji, D. Zhao, J. Liu, W. Zhang, M. Zhu, W. Jie, B.-B. Zhang and Y. Xu, *J. Energy Chem.*, 2022, **66**, 459–465.
16 P. Luo, S. Zhou, W. Xia, J. Cheng, C. Xu and Y. Lu, *Adv. Mater. Interfaces*, 2017, **4**, 1600970.
17 Y. Zhou, K. Fernando, J. Wan, F. Liu, S. Shrestha, J. Tisdale, C. J. Sheehan, A. C. Jones, S. Tretiak, H. Tsai, H. Huang and W. Nie, *Adv. Funct. Mater.*, 2021, **31**, 2101058.
18 R. Quintero-Bermudez, A. Gold-Parker, A. H. Proppe, R. Munir, Z. Yang, S. O. Kelley, A. Amassian, M. F. Toney and E. H. Sargent, *Nat. Mater.*, 2018, **17**, 900–907.
19 Y. Lei, Y. Chen, R. Zhang, Y. Li, Q. Yan, S. Lee, Y. Yu, H. Tsai, W. Choi, K. Wang, Y. Luo, Y. Gu, X. Zheng, C. Wang, C. Wang, H. Hu, Y. Li, B. Qi, M. Lin, Z. Zhang, S. A. Dayeh, M. Pharr, D. P. Fenning, Y.-H. Lo, J. Luo, K. Yang, J. Yoo, W. Nie and S. Xu, *Nature*, 2020, **583**, 790–795.
20 W. Li, H. Li, J. Song, C. Guo, H. Zhang, H. Wei and B. Yang, *Sci. Bull.*, 2021, **66**, 2199–2206.
21 L. Zhao, Y. Zhou, Z. Shi, Z. Ni, M. Wang, Y. Liu and J. Huang, *Nat. Photonics*, 2023, **17**, 315–323.
22 D. Ju, Y. Dang, Z. Zhu, H. Liu, C.-C. Chueh, X. Li, L. Wang, X. Hu, A. K. Y. Jen and X. Tao, *Chem. Mater.*, 2018, **30**, 1556–1565.
23 R. K. Battula, G. Veerappan, P. Bhyrappa, C. Sudakar and E. Ramasamy, *Surf. Interfaces*, 2023, **36**, 7.
24 Z. H. Chen, Q. Zhang, M. L. Zhu, X. Y. Wang, Q. X. Wang, A. T. S. Wee, K. P. Loh, G. Eda and Q. H. Xu, *Adv. Funct. Mater.*, 2020, **30**, 8.
25 Y. C. Liu, Y. X. Zhang, Z. Yang, J. S. Feng, Z. Xu, Q. X. Li, M. X. Hu, H. C. Ye, X. Zhang, M. Liu, K. Zhao and S. Z. Liu, *Mater. Today*, 2019, **22**, 67–75.
26 Y. X. Zhang, Y. C. Liu, Z. Xu, H. C. Ye, Q. X. Li, M. X. Hu, Z. Yang and S. Z. Liu, *J. Mater. Chem. C*, 2019, **7**, 1584–1591.
27 D. Shi, V. Adinolfi, R. Comin, M. J. Yuan, E. Alarousu, A. Buin, Y. Chen, S. Hoogland, A. Rothenberger, K. Katsiev, Y. Losovyj, X. Zhang, P. A. Dowben, O. F. Mohammed, E. H. Sargent and O. M. Bakr, *Science*, 2015, **347**, 519–522.
28 D. Shi, V. Adinolfi, R. Comin, M. Yuan, E. Alarousu, A. Buin, Y. Chen, S. Hoogland, A. Rothenberger, K. Katsiev, Y. Losovyj, X. Zhang, P. A. Dowben, O. F. Mohammed, E. H. Sargent and O. M. Bakr, *Science*, 2015, **347**, 519–522.
29 A. Kanak, O. Kopach, L. Kanak, I. Levchuk, M. Isaiev, C. J. Brabec, P. Fochuk and Y. Khalavka, *Cryst. Growth Des.*, 2022, **22**, 4115–4121.
30 B. Wang, C. Y. Zhang, W. L. Zheng, Q. G. Zhang, Q. Wan, L. Kong and L. Li, *Chem. Commun.*, 2020, **56**, 11291–11294.
31 V. K. LaMer, *Ind. Eng. Chem.*, 1952, **44**, 1270–1277.
32 V. K. LaMer and R. H. Dinegar, *J. Am. Chem. Soc.*, 1950, **72**, 4847–4854.
33 Y. Cho, H. R. Jung and W. Jo, *Nanoscale*, 2022, **14**, 9248–9277.
34 Y. Wu, J. Feng, Z. Yang, Y. Liu and S. Liu, *Adv. Sci.*, 2023, **10**, 2205536.
35 J. X. Hao and X. Xiao, *Front. Chem.*, 2022, **9**, 11.
36 L. Chouhan, S. Ghimire, C. Subrahmanyam, T. Miyasaka and V. Biju, *Chem. Soc. Rev.*, 2020, **49**, 2869–2885.
37 F. L. Binsbergen, *J. Polym. Sci., Part C: Polym. Symp.*, 1977, **59**, 11–29.
38 M. Avrami, *J. Chem. Phys.*, 1940, **8**, 212–224.
39 Y. L. Guo, K. Shoyama, W. Sato, Y. Matsuo, K. Inoue, K. Harano, C. Liu, H. Tanaka and E. Nakamura, *J. Am. Chem. Soc.*, 2015, **137**, 15907–15914.
40 K. Wang, C. C. Wu, D. Yang, Y. Y. Jiang and S. Priya, *ACS Nano*, 2018, **12**, 4919–4929.
41 M. Jung, S. G. Ji, G. Kim and S. I. Seok, *Chem. Soc. Rev.*, 2019, **48**, 2011–2038.
42 P. Barua and I. Hwang, *Materials*, 2023, **16**, 2110.
43 P. K. Nayak, D. T. Moore, B. Wenger, S. Nayak, A. A. Haghighirad, A. Fineberg, N. K. Noel, O. G. Reid, G. Rumbles, P. Kukura, K. A. Vincent and H. J. Snaith, *Nat. Commun.*, 2016, **7**, 13303.
44 J. Chen, D. J. Morrow, Y. Fu, W. Zheng, Y. Zhao, L. Dang, M. J. Stolt, D. D. Kohler, X. Wang, K. J. Czech, M. P. Hautzinger, S. Shen, L. Guo, A. Pan, J. C. Wright and S. Jin, *J. Am. Chem. Soc.*, 2017, **139**, 13525–13532.
45 J. Frenkel, *J. Chem. Phys.*, 1939, **7**, 538–547.
46 A. A. Zhumekenov, V. M. Burlakov, M. I. Saidaminov, A. Alofi, M. A. Hague, B. Turedi, B. Davaasuren, I. Dursun, N. Cho, A. M. El-Zohry, M. De Bastiani, A. Giugni, B. Torre, E. Di Fabrizio, O. F. Mohammed, A. Rothenberger, T. Wu, A. Goriely and O. M. Bakr, *ACS Energy Lett.*, 2017, **2**, 1782–1788.
47 S. Matt, Z. Kun, H. Christopher, H. A. Robert, M. Mischa, H. Andrew, B. R. William, C. Zhengdong, M. Thomas and P. M. Chaikin, *J. Phys.: Condens. Matter*, 2003, **15**, S11.
48 M. R. Singh and D. Ramkrishna, *Chem. Eng. Sci.*, 2014, **107**, 102–113.
49 D. Chakraborty and G. N. Patey, *Chem. Phys. Lett.*, 2013, **587**, 25–29.
50 M. J. Yang, T. Y. Zhang, P. Schulz, Z. Li, G. Li, D. H. Kim, N. J. Guo, J. J. Berry, K. Zhu and Y. X. Zhao, *Nat. Commun.*, 2016, **7**, 9.
51 Z. Yao, W. Wang, H. Shen, Y. Zhang, Q. Luo, X. Yin, X. Dai, J. Li and H. Lin, *Sci. Technol. Adv. Mater.*, 2017, **18**, 253–262.
52 F. Yao, J. L. Peng, R. M. Li, W. J. Li, P. B. Gui, B. R. Li, C. Liu, C. Tao, Q. Q. Lin and G. J. Fang, *Nat. Commun.*, 2020, **11**, 9.
53 B. Li, D. Binks, G. Cao and J. Tian, *Small*, 2019, **15**, 1903613.
54 C. M. Raghavan, T. P. Chen, S. S. Li, W. L. Chen, C. Y. Lo, Y. M. Liao, G. Haider, C. C. Lin, C. C. Chen, R. Sankar, Y. M. Chan, F. C. Chou and C. W. Chen, *Nano Lett.*, 2018, **18**, 3221–3228.
55 K. Y. Yan, M. Z. Long, T. K. Zhang, Z. H. Wei, H. N. Chen, S. H. Yang and J. B. Xu, *J. Am. Chem. Soc.*, 2015, **137**, 4460–4468.
56 Z. Q. Xu, Z. H. Liu, N. X. Li, G. Tang, G. H. J. Zheng, C. Zhu, Y. H. Chen, L. G. Wang, Y. Huang, L. Li, N. Zhou, J. W. Hong, Q. Chen and H. P. Zhou, *Adv. Mater.*, 2019, **31**, 9.
57 J. C. Hamill, J. Schwartz and Y. L. Loo, *ACS Energy Lett.*, 2018, **3**, 92–97.
58 F. Fei, L. Gu, Y. Xu, K. Du, X. Zhou, X. Dong, X. Chen, N. Yuan, S. Wang and J. Ding, *ACS Appl. Mater. Interfaces*, 2022, **14**, 52960–52970.
59 F. Luan, H. Li, S. Gong, X. Chen, C. Shou, Z. Wu, H. Xie and S. Yang, *Nanotechnology*, 2023, **34**, 055402.
60 D. P. Nenon, J. A. Christians, L. M. Wheeler, J. L. Blackburn, E. M. Sanehira, B. Dou, M. L. Olsen, K. Zhu, J. J. Berry and J. M. Luther, *Energy Environ. Sci.*, 2016, **9**, 2072–2082.
61 D. P. McMeekin, Z. P. Wang, W. Rehman, F. Pulvirenti, J. B. Patel, N. K. Noel, M. B. Johnston, S. R. Marder, L. M. Herz and H. J. Snaith, *Adv. Mater.*, 2017, **29**, 8.
62 B. J. Dou, L. M. Wheeler, J. A. Christians, D. T. Moore, S. P. Harvey, J. J. Berry, F. S. Barnes, S. E. Shaheen and M. van Hest, *ACS Energy Lett.*, 2018, **3**, 979–985.

63 W. Zhang, S. Pathak, N. Sakai, T. Stergiopoulos, P. K. Nayak, N. K. Noel, A. A. Haghighirad, V. M. Burlakov, D. W. deQuilettes, A. Sadhanala, W. Z. Li, L. D. Wang, D. S. Ginger, R. H. Friend and H. J. Snaith, *Nat. Commun.*, 2015, **6**, 9.
64 D. Meggiolaro, S. G. Motti, E. Mosconi, A. J. Barker, J. Ball, C. A. R. Perini, F. Deschler, A. Petrozza and F. De Angelis, *Energy Environ. Sci.*, 2018, **11**, 702–713.
65 Y. Liu, X. P. Zheng, Y. J. Fang, Y. Zhou, Z. Y. Ni, X. Xiao, S. S. Chen and J. S. Huang, *Nat. Commun.*, 2021, **12**, 8.
66 L. Ma, Z. G. Yan, X. Y. Zhou, Y. Q. Pi, Y. P. Du, J. Huang, K. W. Wang, K. Wu, C. Q. Zhuang and X. D. Han, *Nat. Commun.*, 2021, **12**, 10.
67 W. M. Gu, K. J. Jiang, Y. Zhang, G. H. Yu, C. Y. Gao, X. H. Fan and L. M. Yang, *Chem. Eng. J.*, 2022, **430**, 7.
68 M. Luo, X. P. Zong, W. H. Zhang, M. N. Hua, Z. Sun, M. Liang and S. Xue, *ACS Appl. Mater. Interfaces*, 2022, **14**, 31285–31295.
69 B. Q. Zhang, C. Chen, X. Z. Wang, X. F. Du, D. C. Liu, X. H. Sun, Z. P. Li, L. Z. Hao, C. Y. Gao, Y. M. Li, Z. P. Shao, X. Wang, G. L. Cui and S. P. Pang, *Angew. Chem., Int. Ed.*, 2023, **62**, 6.
70 X. D. Li, W. X. Zhang, W. J. Zhang, H. Q. Wang and J. F. Fang, *Nano Energy*, 2019, **58**, 825–833.
71 Y. H. Ma, Y. H. Cheng, X. W. Xu, M. L. Li, C. J. Zhang, S. H. Cheung, Z. X. Zeng, D. Shen, Y. M. Xie, K. L. Chiu, F. Lin, S. K. So, C. S. Lee and S. W. Tsang, *Adv. Funct. Mater.*, 2021, **31**, 9.
72 Y. Q. Zhu, Y. X. Liu, B. W. Jin, Y. Shi, Z. X. Wu, J. G. Cao, H. J. Li and C. C. Wu, *Macromol. Mater. Eng.*, 2022, **307**, 9.
73 W. Jiang, J. Ren, H. Li, D. Liu, L. Yang, Y. Xiong and Y. Zhao, *Small Methods*, 2023, **7**, 2201636.
74 C. Park, H. Ko, D. H. Sin, K. C. Song and K. Cho, *Adv. Funct. Mater.*, 2017, **27**, 1703546.
75 S. J. Khanam, N. Parikh, S. Satapathi, A. Kalam, M. Banavoth and P. Yadav, *ACS Appl. Energy Mater.*, 2022, **5**, 14732–14738.
76 M. Wang, X. B. Yin, P. G. Vekilov, R. W. Peng and N. B. Ming, *Phys. Rev. E: Stat. Phys., Plasmas, Fluids, Relat. Interdiscip. Top.*, 1999, **60**, 1901–1905.
77 E. Vlieg, *J. Cryst. Growth*, 2022, **597**, 126850.
78 H. Du, K. Wang, L. Zhao, C. Xue, M. Zhang, W. Wen, G. Xing and J. Wu, *ACS Appl. Mater. Interfaces*, 2020, **12**, 2662–2670.
79 Y. Liu, H. Ye, Y. Zhang, K. Zhao, Z. Yang, Y. Yuan, H. Wu, G. Zhao, Z. Yang, J. Tang, Z. Xu and S. Liu, *Matter*, 2019, **1**, 465–480.
80 E. Hong, Z. Li, T. Yan and X. Fang, *Nano Lett.*, 2022, **22**, 8662–8669.
81 Y. Liu, Q. Dong, Y. Fang, Y. Lin, Y. Deng and J. Huang, *Adv. Funct. Mater.*, 2019, **29**, 1807707.